CRYSTAL GROWTH & DESIGN

Article

pubs.acs.org/crystal

Reticular Growth of Silicon Ridges: Random Walk in Two Dimensions

Sergey N. Dedyulin,* Giovanni Fanchini, and Lyudmila V. Goncharova

Department of Physics and Astronomy, University of Western Ontario, 1151 Richmond Street, London, Ontario, Canada N6A 3K7

Supporting Information

ABSTRACT: We report an observation of arrays of self-assembled Si ridges grown by vapor−liquid−solid mechanism in a molecular beam epitaxy (MBE) chamber. The growth experiments are conducted on Si(100) substrates using Au droplets as seeds for growth of Si ridges. We show that at a sufficiently low flux of Si atoms, gold droplets are propelled forward along two orthogonal ⟨011⟩ directions by the growing silicon ridges. The reticular growth closely resembles a self-avoiding random walk in two dimensions, as we confirmed by using Monte Carlo simulation. The result is a formation of a network of Si ridges with a topological complexity and connectivity that depends on the growth time as well as the starting diameter of the Au droplets. On the basis of our experimental results, we elaborate on the role of diffusion in the MBE growth of Si ridges.

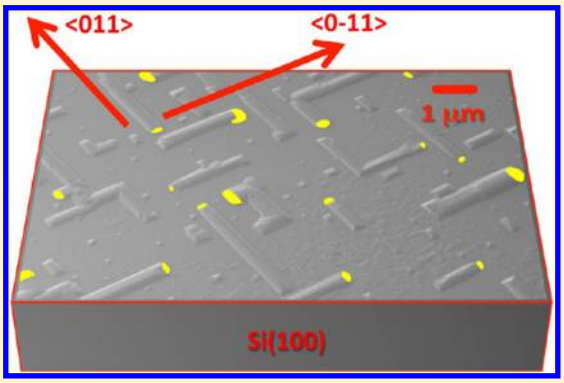

INTRODUCTION

The vapor−liquid−solid (VLS) model was first proposed in the early 1960s[1] and, to date, still remains the most utilized and debated paradigm for modeling the growth of silicon wires. The term vapor−liquid−solid refers to the pathway of silicon during the growth process. According to this model, silicon in the vapor phase impinges on a substrate covered with liquid metallic (nano)particles. Silicon atoms dissolve into the liquid droplets and, when their concentration in the droplet exceeds the saturation point, excess silicon crystallizes as a solid wire at the droplet/substrate interface. In the VLS model, the cross section and crystallographic direction of the wire's growth are controlled by the surface energies at the silicon/gas phase and droplet/silicon interfaces. The underlying assumption is that growth takes place under local thermodynamic equilibrium conditions and in a very small volume close to the droplet/wire interface.[2] Gold is the typical metal of choice for the preparation of the droplets because it is chemically inert and has a eutectic point at low temperature and high silicon solubility.[3]

Under the assumptions mentioned above, minimization of the gold droplet/silicon interface energy dictates that silicon wires of sufficiently large diameter preferentially grow along the ⟨111⟩ silicon crystallographic direction with a hexagonal cross section formed by {110} and {112} facets.[1,4] Conversely, the lateral surface energy contribution dominates over the gold droplet/silicon interface energy for silicon nanowires and wires of a relatively small diameter. Even at the slowest growth rates, surface energy minimization controls the preferential direction of growth, which results in (nano)wires that are oriented along the ⟨110⟩ crystallographic direction,[5−8] with hexagonal cross sections formed by four {111} and two {100} facets.[7,9] High resolution transmission electron microscope experiments indicate that the gold/silicon interface remains oriented along the ⟨111⟩ direction even during ⟨110⟩ growth,[7] with the formation of facets at the gold droplet/silicon interface.

The majority of the reports on VLS growth of oriented silicon wires refer to wires that grow vertically, or tilted with respect to a substrate's normal. This requires further assembling procedures to make planar integrated-circuit devices on the substrates.[6,10−13] To the best of our knowledge, the few existing reports of controlled horizontal growth of silicon wires describe their fabrication in lithographically patterned trenches on Si(110) substrates,[10−12] whereas spontaneous horizontal growth is highly desirable for electronic applications.

In this paper, we report the epitaxial growth of silicon ridges on Si(100) substrates using molecular beam epitaxy. Our three-step growing process involves depositing a uniform Au film of 1 and 2 nm thickness, annealing the Au film to form an array of Au droplets of 90 and 60 nm diameter, respectively, and evaporating Si at 5×10^{14} atoms × cm^{-2} min^{-1} rate for 30−360 min at 650 °C. We believe that the extremely low growth rate in comparison to the chemical vapor deposition (CVD) method is one of the reasons for the observed in-plane growth of Si ridges. Gold droplets are propelled forward along two orthogonal ⟨011⟩ directions and form an orthogonal network of Si ridges with a topological complexity and connectivity that depends on the growth time as well as the starting diameter of the Au droplets. Ostwald ripening of gold droplets offers additional means to control the evolution of ridge's length, as we confirmed by using the Monte Carlo simulations. On the basis of our experimental results, we elaborate on the role of diffusion in the MBE growth of Si ridges and comment on the reasons responsible for lateral growth.

Received: November 15, 2013
Revised: January 16, 2014
Published: February 3, 2014

   dx.doi.org/10.1021/cg4017118 | *Cryst. Growth Des.* 2014, 14, 1193−1198

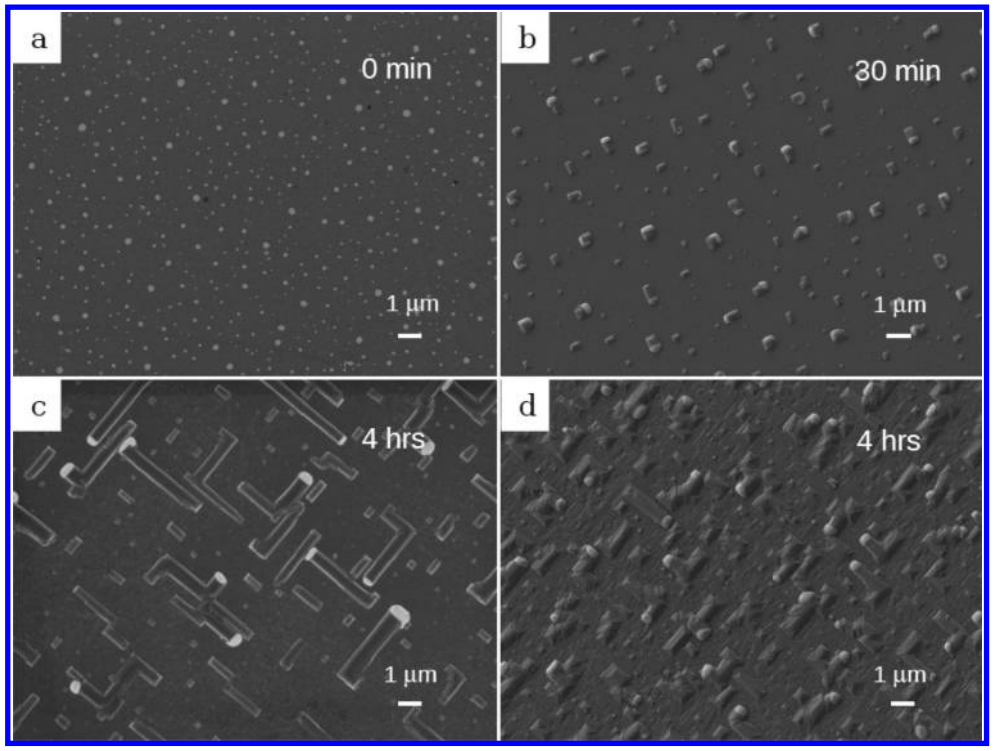

Figure 1. SEM planar views of Si ridges obtained on Si(100) substrate at T = 650 °C using 90 nm Au droplets (a–c) and 60 nm Au droplets (d). The Si deposition times are as indicated on the figures.

EXPERIMENTAL METHODS

Si ridge growth experiments were carried out in an ultrahigh vacuum (UHV) MBE chamber (Kurt Lesker), containing two sources with Si (Alfa Aesar, 99.9999% purity) and Au (Canadian Mint, 99.999% purity), that are evaporated from water-cooled graphite crucibles using electron beam heating. The deposition rate was controlled using the quartz crystal monitors that were calibrated by means of independent Rutherford backscattering measurements. The substrates are heated by an electron beam heater (VG Ltd., Hastings) and their temperature is controlled by K-type thermocouples (OMEGA). Pieces of single-side-polished n-Si(100) wafers (Silicon Valley Microelectronics) of 8 × 10 mm size were used as substrates for our depositions.

Prior to loading the samples in the UHV MBE chamber, the native silicon oxide layer on the substrate was removed by etching for 60 s in an HF buffer solution (Transene Company, Inc.). The substrate was subsequently mounted on a Mo sample holder using indium (Sigma Aldrich, 99.99% purity) as an adhesive and was transferred to the UHV MBE chamber via a load-locking chamber. Any silicon oxide layer that may have been formed during the transfer on the substrates is then removed by outgassing them at 600 °C for 15 min and subsequently heating the substrate at 850 °C for 10 min at 4 × 10^{-9} Torr base pressure prior to the deposition process. After the substrate had cooled to room temperature, thin gold films of 1 or 2 nm thickness were deposited at 4 × 10^{15} atoms × cm^{-2} min^{-1} growth rate on the Si(100) wafers. Substrates covered with 1 or 2 nm Au film were annealed at 650 °C for 30 min in order to form gold droplets of 90 or 60 nm diameter, respectively. These droplets served as a catalyst for the growth of the ridges. The reported values correspond to the maximum of gold droplet size distribution. Si was deposited at 5 × 10^{14} atoms × cm^{-2} min^{-1} rate for 30–360 min at 650 °C and (1–2) × 10^{-8} Torr pressure.

The Si ridges were analyzed by using different scanning electron microscopes: a LEO (Zeiss) 1530 SEM and a LEO (Zeiss) 1540 XB FIB/SEM. The Monte Carlo simulation program for modeling the growth of Si ridges has been written in Python (version 2.6.5) and is described in detail in the Supporting Information.

RESULTS AND DISCUSSION

In our MBE system, we carried out a set of growth experiments by changing two relevant parameters: the time of growth (30–360 min) and the average thickness of the Au thin film (1 or 2 nm). Upon annealing, 1 nm Au films formed droplets of 90 nm diameter with an average separation Δr_{avg} = 409 ± 96 nm and areal density of 2.336 × 10^{-6} nm^{-2}. In comparison, 2 nm Au films formed droplets of 60 nm diameter with an average separation Δr_{avg} = 262 ± 86 nm and areal density of 7.190 × 10^{-6} nm^{-2}. Droplet-covered substrates were exposed to a uniform flux of silicon atoms for various length of time.

If the system is limited by transport phenomena, then adsorption of a silicon atom from the vapor phase onto a Si(100) wafer may result in two competing outcomes. The first possibility is the growth of epitaxial silicon layers by island coalescence[14] which takes place if the surface diffusion length of silicon atoms, L_D, is much smaller than the average distance between the gold droplets, $L_D \ll \Delta r_{avg}$. The second possible outcome is dissolution of the silicon adatoms into a gold droplet which takes place if $L_D \sim \Delta r_{avg}$. At the specific temperature of 650 °C and a low Si flux of 5 × 10^{14} atoms × cm^{-2} min^{-1} optimized in the present work, the diffusion length of the adatoms exceeds L_D = 200 nm.[15,16] Under these conditions, the growth proceeds by preferential incorporation of silicon into gold droplets for both 1 nm and 2 nm Au films because L_D and Δr_{avg} have the same order of magnitude. In accordance with the VLS growth model, liquid droplets then capture material from the vapor and deposit it onto the solid in the form of ridges (Figure 1), with longer silicon deposition time resulting in longer ridges.

The ridges have a width that is determined by the diameter of the Au droplets. If the size and shape of the droplets do not change during the growth process, one would expect the final distribution of the width of the silicon ridges to reflect the

dx.doi.org/10.1021/cg4017118 | Cryst. Growth Des. 2014, 14, 1193–1198

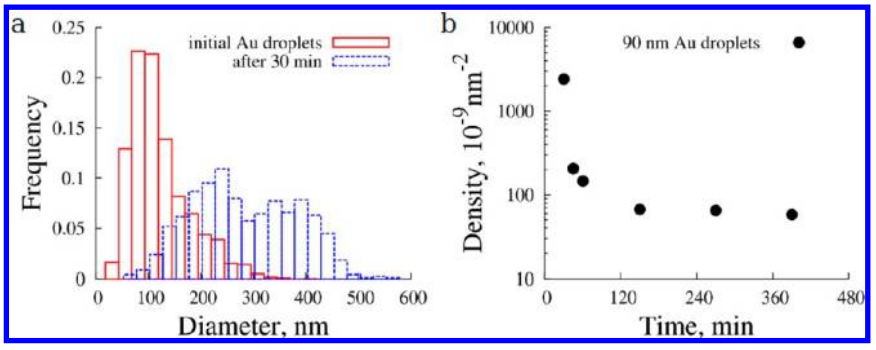

Figure 2. Ostwald ripening of 90 nm Au droplets. (a) Changes in the gold droplet diameter after 30 min of silicon deposition. Initial single-peak size distribution of the gold droplets (maximum at 90 nm) becomes distinctly bimodal. (b) Decrease in the areal density of gold droplets as a function of growth time.

initial distribution of the gold particle diameters. In addition, the final areal density of the silicon ridges should be equal to the initial areal density of the gold droplets. Figure 2 shows that this is not the case. Panel a in this figure reports the ridge width distribution after 30 min of Si deposition. Panel b reports the average gold droplet areal density as a function of time. Even after 30 min of growth, when ridges are less than 1 μm long and not colliding with each other, the diameters of silicon ridges are much larger than the initial Au droplet diameters. This suggests that significant Ostwald ripening[17] of the droplets, a process in which larger gold droplets ripen at the expense of the smaller ones, has taken place. This conclusion is further supported by observing that the gold areal density is inversely proportional to the growth time (Figure 2b).

We argue that Ostwald ripening is responsible for the roughening of the Si film between the Si ridges in the case of 60 nm Au droplets (Figure 1d). The smaller relative size and higher areal density of the droplets formed upon anneal of 2 nm Au film lead to the formation of multiple small silicon ridges in between the larger ones. During the growth, small gold droplets at the tip of those small ridges evaporate as a result of Ostwald ripening, leaving behind small silicon islands. Growth and coarsening of these islands causes rough Si film to grow on the substrate surface.

For the CVD growth by the VLS mechanism, it is well-known that wires with larger diameter Au droplet at the tip should grow faster than those with smaller diameter droplet due to the Gibbs-Thompson effect.[2] In contrast, we observe in our MBE experiments the opposite trend: thinner ridges grow faster than thicker ones as shown in Figure 3. Similar results were obtained for the MBE growth of vertical Si wires on Si(111) substrates[18] and explained theoretically by incorporating surface diffusion of silicon into the VLS growth model.[19] Additional experimental evidence of the role of diffusion in the MBE growth of Si ridges is discussed further below. Note: broad length distribution of silicon ridges might be caused by complex growth dynamics. Multiple turns and collisions between the ridges can result in the redistribution of Au at the tip of the growing ridge which in turn will cause changes in its growth rate.

Our observations indicate that low silicon flux rate and Si(100) substrate morphology are crucial factors in the growth of silicon ridges. First, increasing the silicon flux to 1.3×10^{16} atoms $\times$ cm^{-2} min^{-1} leads to Si layer growth by island coalescence as shown in Figure 4. Under these conditions, the areal density of silicon adatoms on the surface is high enough to allow nucleation of multiple stable silicon islands in between

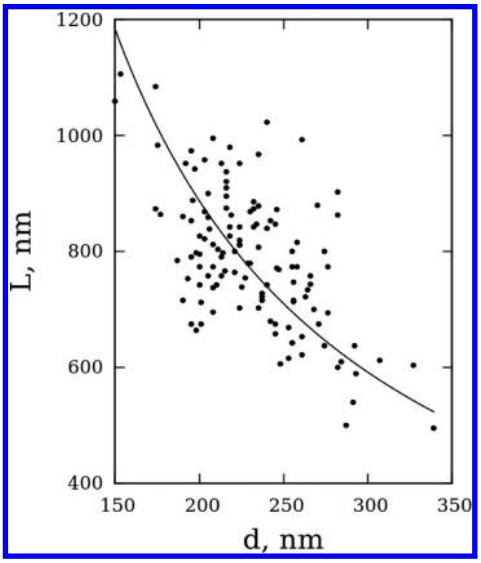

Figure 3. Correlation between the length L and width d of Si ridges. In this specific case, the growth experiment was performed at temperature $T = 650$ °C and flux $F = 5 \times 10^{14}$ atoms $\times$ cm^{-2} min^{-1} for 1 h using 90 nm Au droplets. The solid line is the least-squares fit to the function Cd^{-1}, where C is a constant, predicted by the 'diffusion-droplet' model.[19]

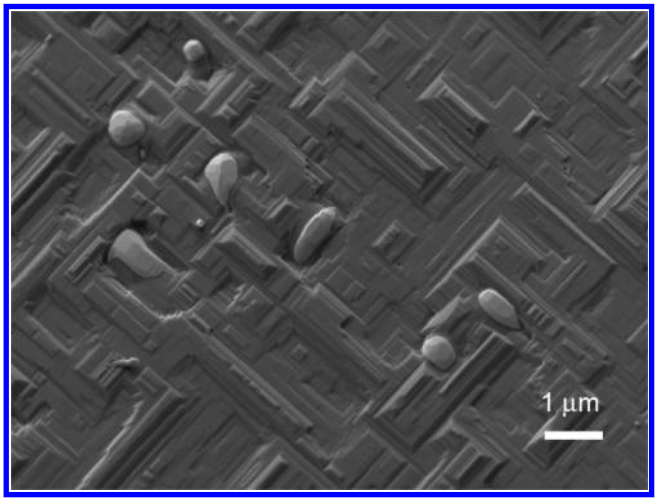

Figure 4. SEM micrograph of a diffusion limited growth of Si ridges using 60 nm Au droplets. The growth temperature $T = 650$ °C and flux $F = 1.3 \times 10^{16}$ atoms $\times$ cm^{-2} min^{-1}.

dx.doi.org/10.1021/cg4017118 | Cryst. Growth Des. 2014, 14, 1193−1198

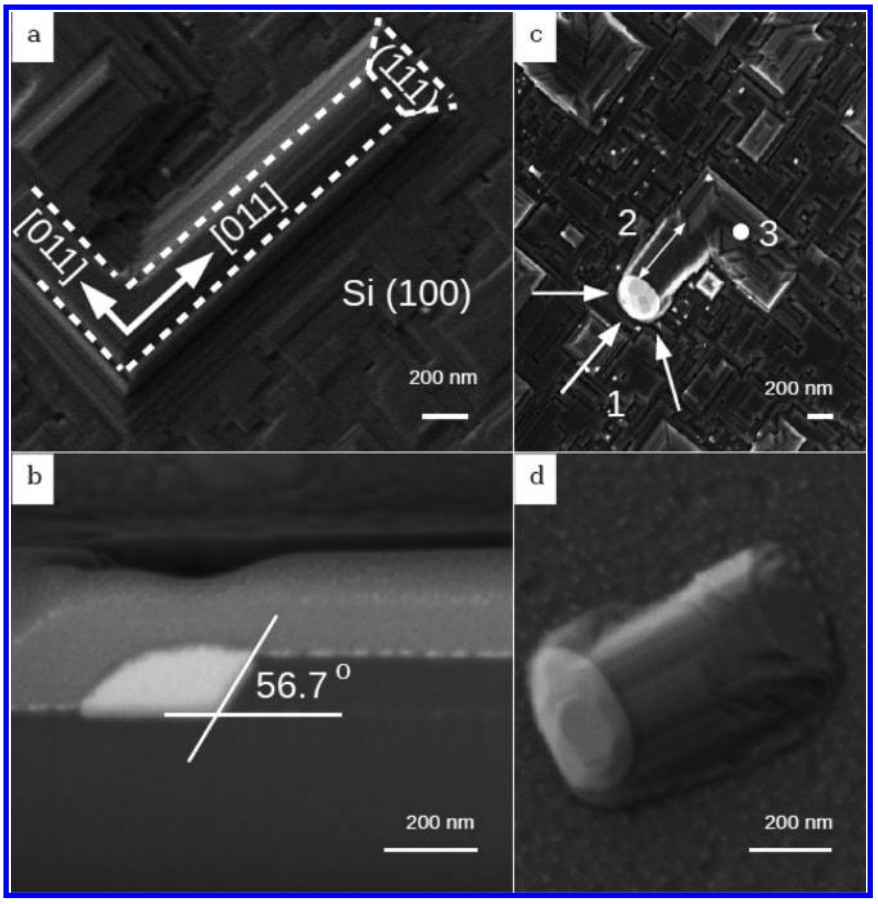

Figure 5. Individual silicon ridge shape and orientation. (a) SEM micrograph of Si ridge facets. (b) High resolution SEM image of the Si ridge cross-section along the growth direction. (c) SEM image of the Si ridge after 4 h silicon deposition. Arrows indicate the following: 1, surface diffusion of Si adatoms on Si(100) substrate; 2, the region of the silicon ridge where the Si surface diffusion dominates; 3, the region of the silicon ridge where the bulk diffusion dominates. (d) SEM planar view of Si ridge after 30 min silicon deposition.

the Au droplets. Growth and coarsening of these islands causes rough Si film to grow. Second, using Si(111) substrates in a similar MBE deposition system[18,20,21] resulted in the growth of vertically aligned silicon wires.

We attribute this behavior to the impact of the surface energy of the ridge's facets and their growth rate on the stability of vapor−liquid−solid trijunction of the growing wire, as it has been previously considered in the 2D continuum model.[22,23] The model captures many experimentally observed (nano)wire morphologies, including kinking from one direction to another for the vertical wires or crawling along the surface.

In this 2D continuum model, lateral growth is initiated when the liquid droplet rolls off the tapered (nano)wire base due to failed edge formation at the transition from the tapering pedestal to a uniform wire.[23] Difficulty in introducing new facets can be affected by absorbed gases, growth temperature, impurities, and so forth. We speculate that this failure of edge formation may be related to the observed faceting of ridges sidewalls (see Supporting Information for details). In addition, simulations in the 2D continuum model suggest that the growth rate can strongly affect the occurrence of kinking and crawling.[23]

As it was mentioned before, the ridge growth rate is very slow, about 900 nm/h for the longest ridges at silicon atom flux $F = 5 \times 10^{14}$ atoms $\times$ cm^{-2} min^{-1}. We argue that this slow growth rate ensures epitaxial growth of Si ridges on Si(100) substrate. The ridges are aligned with Si ⟨011⟩ crystallographic direction with occasional turns at 90° primarily caused by a collision with another ridge at the later stages of growth. In Figure 5a, we show a single Si ridge with a schematically drawn orientation for ridge surfaces. The ⟨011⟩ axes have been assigned based on the known crystallographic orientation of the original Si substrate with respect to the ridge growth directions (see Supporting Information). The Au liquid−solid interface is ⟨111⟩-oriented as follows from the analysis of a cross-sectional SEM image of an individual silicon ridge along the direction of growth (Figure 5b). This observation agrees with the predictions of the VLS model for large diameter silicon ridges. However, the silicon ridges maintain a semicircular cross section for the first 0.5−1 μm from the gold droplets (Figure 5c, d). This disagrees with the VLS model which predicts a faceted shape of the wire cross section dominated by {110} or {112} facets. In our case, ridges assume faceted cross sections only at relatively large distances, r, from the droplets, $r > L_D$. This behavior underlines the critical role of a surface diffusion in our growth process. If the length of the ridge is smaller than the surface diffusion length of Si adatoms on the Si(100) surface, the ridge maintains a semicircular cross section through its entire length (Figure 5d).

To further elucidate the mechanism responsible for reticular growth of silicon ridges, we performed Monte Carlo simulations of ridge length evolution as a function of silicon deposition time (see Supporting Information for the details of the code). We have modeled the behavior of individual ridges

dx.doi.org/10.1021/cg4017118 | Cryst. Growth Des. 2014, 14, 1193−1198

according to the rules of self-avoiding random walk in two dimensions.[24] The individual walker is randomly placed on a 2D square lattice and allowed to go in one of the two orthogonal directions. Once chosen, the direction of the walk and step size are kept fixed until the walker intercepts another walk path. At that point, there is a chance for the walker to turn left or right from the direction it was following or to stop. The probabilities for each particular outcome of the collision are determined from counting statistics after 4 h of silicon deposition. The individual steps in the simulation correspond to 10 min of silicon deposition. The important parameters, such as the areal density of the walkers and the average distance between the walkers or the average step size, were taken from the experiment after 0 or 30 min of silicon deposition, respectively. We have also introduced a decaying termination rate in order to simulate the effects of Ostwald ripening: at each step, the random walker has a chance to stop which is inversely proportional to the total walk length.

Figure 6 shows schematically four walkers following the rules of self-avoiding random walk in two dimensions after the first

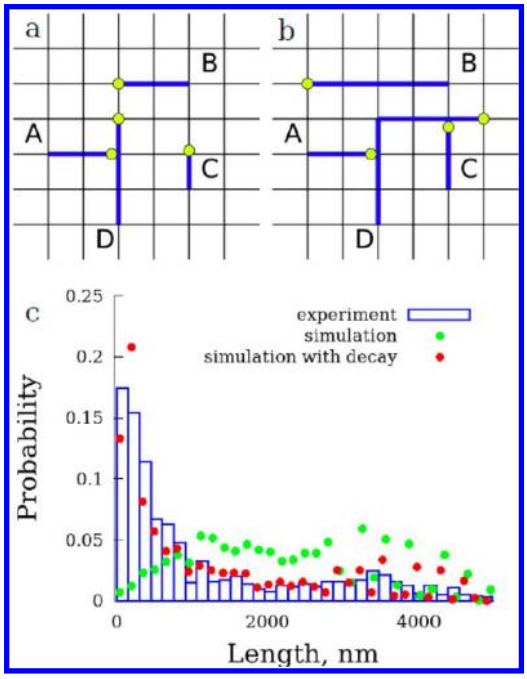

Figure 6. A Monte Carlo simulation of Si ridge growth. Schematics illustrating the rules for Monte Carlo simulations: (a) after the first step and (b) after the second step. (c) The Si ridge length distribution after 4 h of silicon growth (90 nm Au droplets): experimental and Monte Carlo simulation results. For the simulation, the result without a rule that postulates a decay in walkers' areal density, inversely proportional to the walk length, is shown for comparison.

(Figure 6a) and second step (Figure 6b). In this example, the random walk step length is 2 squares per step for walker A, 2 squares for walker B, 1 square for walker C and 4 squares for walker D, which corresponds to the average value of 2 squares per step. The randomly chosen initial directions of the walk are as follows: walker A, to the right; walker B, to the left; walker C and D, up. Since at the second step, the paths of walkers A and D would intercept the paths of walkers D and B, respectively, the following outcomes of the collision are randomly chosen: walker A, termination; walker D, turn right in order to avoid the collision. Figure 6c compares experimental and Monte Carlo simulation results for Si ridge length distribution after 4 h of Si deposition. The self-avoiding random walk combined with the termination of the ridges due to Ostwald ripening describes well the experimental distribution of silicon ridge lengths. Collisions between the ridges with termination as a result of the collision cannot alone contribute to the peak at small ridge lengths. Thus, gold loss plays an important role in the ridge growth mechanism. This issue should be addressed as a means to support the growth of longer ridges. Note: frequent drops in simulated probability values for longer ridges are due to fixed discrete size of random walk steps. Decreasing the size of the step, which is equivalent to increasing the time resolution, will make the simulated results smoother, but at the same time will increase the computational cost.

In summary, the epitaxial growth of silicon ridges by MBE was observed on Si(100) substrates. It is shown that for sufficiently long silicon deposition times, the ridges form a two-dimensional network on the substrate surface which can be successfully simulated by a self-avoiding random walk in two dimensions if the effects of Ostwald ripening are properly taken into account. Due to the peculiarity of MBE growth, our silicon ridges maintain semispherical cross section in the vicinity of the gold droplets, a manifestation of the surface diffusion of silicon atoms.

■ ASSOCIATED CONTENT

Supporting Information

SEM and AFM images with analysis of a growth direction of Si ridges and orientation of ridge facets; statistical analysis of Si ridge collisions and Ostwald ripening of gold droplets; Monte Carlo simulation details. This material is available free of charge via the Internet at http://pubs.acs.org.

■ AUTHOR INFORMATION

Corresponding Author

*Address: Department of Physics and Astronomy, UWO, 1151 Richmond St., London, ON, Canada, N6A 3K7. Phone: 1(519) 661-2111 × 83803. E-mail: sdedyuli@uwo.ca.

Funding

Funding was provided from NSERC, CFI and the University of Western Ontario.

Notes

The authors declare no competing financial interest.

■ ACKNOWLEDGMENTS

We gratefully acknowledge the Nanofabrication Facility (University of Western Ontario) for SEM measurements; Jack Hendriks (Tandetron Lab, University of Western Ontario) for help with MBE chamber; Gabe Keenleyside for help with statistical analysis of SEM images; Arash Akbari-Sharbaf for the help with AFM imaging.

■ ABBREVIATIONS

CVD, chemical vapor deposition; MBE, molecular beam epitaxy; SEM, scanning electron microscopy; UHV, ultra high vacuum; VLS, vapor−liquid−solid

■ REFERENCES

(1) Wagner, R. S.; Ellis, W. C. *Appl. Phys. Lett.* **1964**, *4*, 89−90.
(2) Givargizov, E. I. In *Highly Anisotropic Crystals*; 1st ed.; D. Reidel Pub. Co.: Boston, MA, 1987; pp 70−230.

(3) Schmidt, V.; Wittemann, J. V.; Senz, S.; Gösele, U. *Adv. Mater.* **2009**, *21*, 2681−2702.
(4) Weyher, J. *J. Cryst. Growth* **1978**, *43*, 235−244.
(5) Givargizov, E. I.; Sheftal', N. N. *J. Cryst. Growth* **1971**, *9*, 326−329.
(6) Cui, Y.; Lieber, C. M. *Science* **2001**, *291*, 851−853.
(7) Wu, Y.; Cui, Y.; Huynh, L.; Barrelet, C.; Bell, D. C.; Lieber, C. M. *Nano Lett.* **2004**, *4*, 433−436.
(8) Schmidt, V.; Senz, S.; Gösele, U. *Nano Lett.* **2005**, *5*, 931−935.
(9) Ma, D. D. D.; Lee, C. S.; Au, F. C. K.; Tong, S. Y.; Lee, S. T. *Science* **2003**, *299*, 1874−1877.
(10) Islam, M. S.; Sharma, S.; Kamins, T. I.; Williams, R. S. *Nanotechnology* **2004**, *15*, L5−L8.
(11) He, R.; Gao, D.; Fan, R.; Hochbaum, A. I.; Carraro, C.; Maboudian, R.; Yang, P. *Adv. Mater.* **2005**, *17*, 2098−2102.
(12) Kim, D. R.; Lee, C. H.; Zheng, X. *Nano Lett.* **2010**, *10*, 1050−1054.
(13) Quitoriano, N. J.; Wu, W.; Kamins, T. I. *Nanotechnology* **2009**, *20*, 145303−1−7.
(14) Kolasinski, K. W. In *Surface Science: Foundations of Catalysis and Nanoscience*; 2nd ed.; John Wiley&Sons Ltd.: Mississauga, ON, Canada, 2008; pp 345−351.
(15) Nielsen, J.-F.; Pelz, J. P.; Hibino, H.; Hu, C.-W.; Tsong, I. S. T. *Phys. Rev. Lett.* **2001**, *87*, 136103−1−4.
(16) Lim, S.-H.; Song, S.; Park, T.; Yoon, E.; Lee, J.-H. *J. Vac. Sci. Technol., B* **2003**, *21*, 2388−2392.
(17) Cao, G. In *Nanostructures & Nanomaterials: Synthesis, Properties & Applications*; Imperial College Press: London, 2004; pp 17−32.
(18) Schubert, L.; Werner, P.; Zakharov, N. D.; Gerth, G.; Kolb, F. M.; Long, L.; Gosele, U.; Tan, T. Y. *Appl. Phys. Lett.* **2004**, *84*, 4968−4970.
(19) Johansson, J.; Svensson, C. P. T.; Mårtensson, T.; Samuelson, L.; Seifert, W. *J. Phys. Chem. B* **2005**, *109*, 13567−13571.
(20) Werner, P.; Zakharov, N. D.; Gerth, G.; Schubert, L.; Gosele, U. *Int. J. Mater. Res.* **2006**, *97*, 1008−1015.
(21) Sivakov, V.; Andra, G.; Gösele, U.; Christiansen, S. *Phys. Status Solidi A* **2006**, *203*, 3692−3698.
(22) Schwarz, K. W.; Tersoff, J. *Phys. Rev. Lett.* **2009**, *102*, 206101−1−4.
(23) Schwarz, K. W.; Tersoff, J. *Nano Lett.* **2011**, *11*, 316−320.
(24) Giordano, N. J. In *Computational Physics*; Prentice-Hall Canada, Inc.: Toronto, 1997; pp 232−253.